MDPI

Article

Adaptive SNN for Anthropomorphic Finger Control

Mircea Hulea *[ID], **George Iulian Uleru and Constantin Florin Caruntu** [ID]

Faculty of Automatic Control and Computer Engineering, Gheorghe Asachi Technical University of Iasi, 700050 Iasi, Romania; george-iulian.uleru@academic.tuiasi.ro (G.I.U.); caruntuc@ac.tuiasi.ro (C.F.C.)
* Correspondence: mhulea@tuiasi.ro

Abstract: Anthropomorphic hands that mimic the smoothness of human hand motions should be controlled by artificial units of high biological plausibility. Adaptability is among the characteristics of such control units, which provides the anthropomorphic hand with the ability to learn motions. This paper presents a simple structure of an adaptive spiking neural network implemented in analogue hardware that can be trained using Hebbian learning mechanisms to rotate the metacarpophalangeal joint of a robotic finger towards targeted angle intervals. Being bioinspired, the spiking neural network drives actuators made of shape memory alloy and receives feedback from neuromorphic sensors that convert the joint rotation angle and compression force into the spiking frequency. The adaptive SNN activates independent neural paths that correspond to angle intervals and learns in which of these intervals the rotation the finger rotation is stopped by an external force. Learning occurs when angle-specific neural paths are stimulated concurrently with the supraliminar stimulus that activates all the neurons that inhibit the SNN output stopping the finger. The results showed that after learning, the finger stopped in the angle interval in which the angle-specific neural path was active, without the activation of the supraliminar stimulus. The proposed concept can be used to implement control units for anthropomorphic robots that are able to learn motions unsupervised, based on principles of high biological plausibility.

Keywords: spiking neural networks; neuromorphic hardware; Hebbian learning; anthropomorphic finger

1. Introduction

In the biological world, information is processed using impulses or spikes that provide living creatures with the ability to be aware of the surrounding environment and to act accordingly. For most of the aspects of life, they still outperform conventional, state-of-the-art, robots in terms of speed and energy efficiency [1]. Modelling the motor skills of the human hand and fingers represents a challenging task in robotics, due to the smoothness and diversity of natural motions. The design of control devices for such robotic hands should be based on modelling the behaviour of motor neural areas (MNA) and their bidirectional communication with the muscles. The natural MNA stimulates the muscles through efferent neural pathways that include the motor cortex and the central pattern generators. In the opposite direction, the MNA receives information from spindles about the muscle stretch during relaxation [2] through afferent pathways, and from the Golgi tendon organs during contraction [3]. Considering that the frequency generated by the spindles increases with the muscle stretch by an external force [4], the spindle output can be used to determine the rotation angle of articulation. However, this function cannot be applied when the muscle contracts, because the spindle response to acceleration dominates their response during a passive stretch [5]. When the muscles contract, the Golgi organs respond to the force applied to the tendons, providing information about the muscle activity [6]. Physiological evidence shows that the spindle response is stronger during adaptation tasks, implying that the spindle activity is affected during learning [7,8]. The

detailed mechanisms that provide the basal ganglia with the ability to coordinate automatic movements and to adapt were presented in a recent study [9].

Starting from physiological principles and taking into account the increased interest in robotic control using adaptive spiking neural networks (SNNs) [1], in this paper, we present a biologically plausible structure of spiking neurons that is able to control the rotation of a robotic junction and adapt to custom angles of rotation. Note that the goal of this paper is to demonstrate the proposed concept using a reduced number of electronic neurons and not to reproduce the complexity of the biological neural structures in the basal ganglia [9].

The spiking neural network is based on an artificial neuron model of biological inspiration implemented in analogue hardware [10,11]. Electronic circuits represent a better alternative to model the behaviour of biological neurons because this neuromorphic hardware has the main advantages of the natural neurons, such as fully parallel operation and information transmission. Moreover, the variation of internal signals in an infinite range allows the implementation of very complex functions using a reduced number of neurons. Besides these physical similarities between the natural neurons and their electronic models, the latter benefit from very low power consumption and high reliability.

To achieve the smoothness and accuracy of natural motions, artificial muscles should mimic the behaviour of muscular fibres. Thus, in this work, the artificial muscles are implemented with shape memory alloy (SMA) wires that actuate by contraction, as do biological muscles [12–14], and their contraction strength can be determined directly by the frequency of the electronic spiking neurons [15,16]. The results reported previously [17] show that, despite the slowness and nonlinearity of SMA wires [18], a small SNN with a bioinspired structure [19] is able to control the rotation angle of a SMA-actuated robotic joint when the arm moves towards target positions. In that case, the spiking neural network behaves as a regulator for the rotation angle, even when the arm is slightly loaded. Moreover, a similar SNN structure can be used as a regulator for the force of SMA actuators when a force sensor (FS) replaces the angle sensor (AS) [20].

2. Related Works

Research done until now shows that the contraction of the SMA actuators can be controlled using programmed microcontrollers [21]. Additionally, adaptive SNNs of high biological plausibility were used to control the robotic hands and fingers which were typically actuated by motors [22,23]. The control of SMA actuators using SNNs with fixed weights (non-adaptive) was approached for the first time by our research group [15,16]. As a continuation of this research, the current work presents a new and improved adaptive SNN of high biological plausibility that uses Hebbian learning mechanisms to adapt to custom rotation angles of the robotic junctions.

2.1. SMA Actuators

Actuators made of shape memory alloy are suitable for the actuation of anthropomorphic robotic hands [22,24] and other bioinspired systems [14] such as an artificial jellyfish [25], artificial fingers [26], insect legs [27], and wings [28]. Also, various small scale robots are built with Smart Composite Microstructures (SCM) actuated by SMA actuators [29].

2.2. Adaptive SNNs

Recently, spiking neural networks have gained a special interest due their performance, reduced signal to noise ratio, and lower power consumption comparative to artificial neural networks (ANNs) [30]. Among the characteristics of the SNN, significant attention is given to their complex adaptability mechanisms [31–34], which rigorously model the plasticity rules of the biological synapses such as spike timing-dependent plasticity (STDP) [35–38], input timing-dependent plasticity (ITDP) [39] and homeostasis [40]. Considering that in most practical applications, ANNs show very good performance, several works focus on the

conversion of ANNs to SNNs [30]. Also, high performance deep SNNs were implemented with several learning methods [41–43] including gradient descent [44,45]. Other learning methods were developed for the detection of spatio-temporal patterns [46,47] and for evolving SNN [48].

2.3. SNNs in Robotics

Artificial neural networks were used to describe self-organizing neural models for hand-eye coordination using endogenously generated movement commands correlated with visual, spatial, and motor information to learn internal coordinate transformation [49]. Correlation-based navigation algorithms using STDP learning mechanisms for unsupervised learning were also used to increase the behavioural capabilities of bio-inspired hybrid robots [50]. Robotic arm capability up to 4 degrees of freedom was obtained using an initial period of motor babbling using a spiking neural network architecture that learned autonomously and was simulated according to Izhikevich's model to exhibit biologically realistic behaviour [23].

In order to apply robot manipulators to a wide class of tasks, it is necessary to control the force exerted by the end-effector on the object along the position of the end-effector. The control of the robot manipulators in the task space was designed with an adaptive neural network based on the inverse dynamic model [51]. The issue of ANN performance in solving inverse kinematics was also approached by the inclusion of the feedback of the current joint angle configuration of robotic arm as well as the desired position and orientation in the input pattern of neural network [52]. There are also studies for determining the Jacobian matrix without knowledge of the forward kinematics of a robotic arm, as well as modifying the Jacobian transpose method to achieve better control stability [53]. Another workaround to avoid the complexity of calculating inverse kinematics and doing motion planning is to use a combination of motor primitives where a SNN may be used to represent motions in a hierarchy of such primitives. Correction primitives may be combined using an error signal to control a robot arm in a closed-loop scenario [54]. To achieve guaranteed tracking control and estimation, an adaptive neural control based on a radial basis function neural network (RBFNN) was also proposed for neural network (NN) weight convergence [55].

2.4. Adaptive SNN for Motion Control

A reinforced learning mechanism process was used on an artificial motor cortex based on spiking neurons [56]. Using an output that was partially driven by Poisson motor babbling, analogous to the biological dopamine system, a global reward or punishment signal was provided in response to decreasing or increasing the distance from the hand to the target. Dopamine-modulated STDP was also used in an insular cortex model able to detect tactile patterns [57–59]. Reinforcement learning for a target reaching task, which can be modelled as partially observable Markov decision processes, may extend the proximal policy optimization using a liquid state machine (LSM) for state representation to achieve better performance [60]. Another example of a learning mechanism based on long-term synaptic plasticity was implemented using the temporal difference learning rule to enable the robot to learn to associate the correct movement with the appropriate input conditions [61]. Another method was also approached, which consists of training a neuromorphic controller online modelled by a leaky integrate-and-fire (LIF) SNN to follow a linear quadratic regulator (LQR) controller with known performance guarantees [62]. Similar work has been accomplished by designing a hierarchical SNN with a bio-inspired architecture for representing different grasp motions. Both the hand and the finger networks were trained independently using STDP, incorporating a mechanism for tactile feedback in the finger networks to stop the motion on contact. For the encoding, values were converted into spikes using a mixture of Gaussian kernels to tune the firing rate of a population.

Conventional electrical motors were used in [22] for implementing a robotic hand. Another recent paper presents a biomimetic 2-degrees of freedom (DOF) SMA-actuated

robotic arm which uses a proportional-integral-derivative (PID) controller to enable closed-loop control of the joint angular positions to prove the technology's performance against existing commercial DC motor rotary joints [21].

2.5. Proposed Concept

The novelty presented in this paper is the structure of an adaptive electronic SNN that is able to learn to rotate the index finger towards the angle intervals where its rotation was blocked previously by an external force. To achieve this goal, the SNN encodes the angle intervals by balancing the excitatory and inhibitory activity and potentiates, using Hebbian learning, the neural paths that correspond to the angle at which the finger was stopped. The proposed adaptive SNN is suitable for being implemented in anthropomorphic robots that are able to learn motions unsupervised in a highly biologically plausible manner. The validation of the proposed concept was performed by physical implementation of a robotic hand with an active index finger. The finger is controlled by the SNN using the feedback from the neuromorphic sensors that convert the joint rotation angle and the compression force into spiking frequency.

The rest of the paper is organized as follows: Section 3 presents the general structure of the bioinspired system focusing on the proposed concept of the adaptive SNN that is validated by simulation in Section 4. The testbed for the evaluation of the proposed SNN architecture is presented in Section 5, which also includes the experimental results and the discussion. The paper ends with Section 6, which discusses the utility of this concept and future research directions.

3. Bioinspired System Design

In order to investigate the performance of the adaptive spiking neural network in controlling the rotation of the robotic junctions, we implemented the robotic hand with active index finger presented in Figure 1.
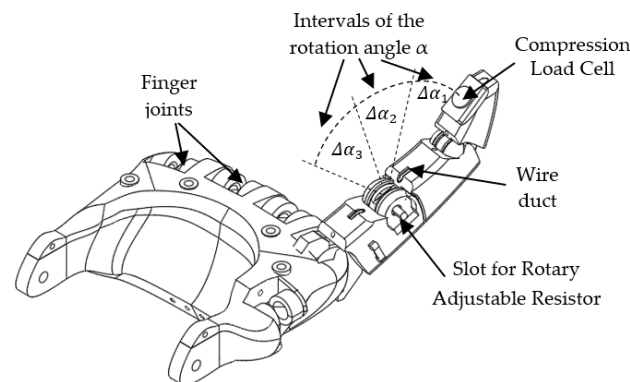

Figure 1. The structure of the anthropomorphic finger.

3.1. Artificial Finger

The metacarpophalangeal joint of the robotic finger can be flexed using a SMA actuator. The rotation angle of this joint is converted into voltage by a rotary adjustable resistor (RAR), while the pressure on the finger apex is sensed by a compression load cell (CLC) as in Figure 1.

To protect the finger from heating, the SMA wire is connected near the wrist to a thread that goes towards the apex of the finger. The finger can be blocked by an external force anywhere in the rotation range that includes the angle intervals $\Delta\alpha_1$, $\Delta\alpha_2$, and $\Delta\alpha_3$. These angle intervals are delimited by the SNN because it activates one neural path when the finger is in each interval, as we will detail below.

3.2. The Structure of the Adaptive SNN

The spiking neural network presented in Figure 2 is able to learn the intervals where

the finger is blocked by an obstacle. To achieve this goal, the neural structure was designed to activate one inhibitory neuron from the inhibitory area (IA) in each of the three sub-SNNs corresponding to angle intervals $\Delta\alpha_1$, $\Delta\alpha_2$ and $\Delta\alpha_3$ (see Figure 2a). When the finger reaches the obstacle, the force sensor activates the excitatory neurons E_1^{FS}, E_2^{FS} and E_3^{FS} that reduce the activity of motor neurons M_1 and M_2 through the inhibitory neurons I_1, I_2, and I_3, respectively.
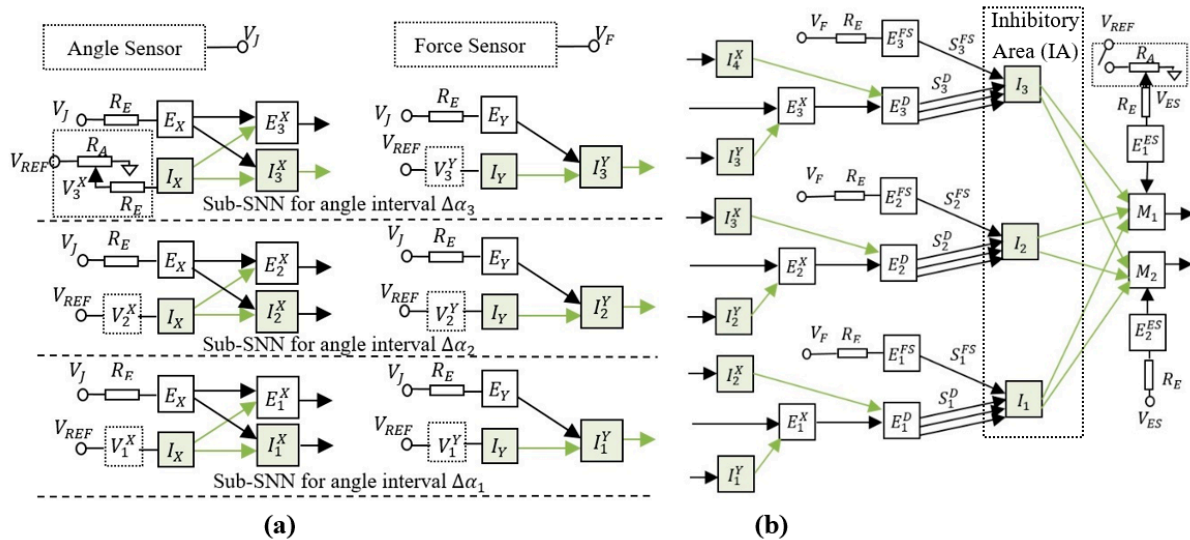

Figure 2. The adaptive neural structure which can be trained using associative learning mechanisms to stop the finger in three subintervals of the rotation range; (**a**) the encoding layers include input neurons E_X, E_Y (excitatory) and I_X, I_Y (inhibitory) that activate a subset of outputs for each rotation interval $\Delta\alpha_{1-3}$; (**b**) the decoding layers used to activate one of the excitatory neurons E_{1-3}^D and adjust the weights of the synapses S_{1-3}^D accordingly; the switch determines the activation of the input neurons $E_{1,2}^{ES}$ and, consequently, of the motor neurons $M_{1,2}$.

Only one of the neurons E_1^D, E_2^D, or E_3^D is active at the same time, depending on the angle interval in which the finger is rotated. The role of these excitatory neurons is to activate one of the inhibitory neurons that stops the finger in the corresponding angle interval. Note that, if more excitatory neurons would be activated, the finger would stop at the first angle interval it reaches. According to the principles of Hebbian learning, the concurrent activation of more synapses determines their potentiation when the postsynaptic neuron is activated. In this case, the concurrent activation of the potentiated synapses S_i^{FS}, $i = \overline{1,3}$ (activated by FS) with the corresponding un-potentiated synapses S_i^D (activated when the arm is in the angle interval $\Delta\alpha_i$) determines the potentiation of S_i^D because the neuron E_i^{FS} activates the postsynaptic neuron I_i. Note that, before training, all synapses except S_i^D have the maximum weights, implying that they determine the activation of the stimulated postsynaptic neurons.

An important structural characteristic of the SNN is related to how the neurons perform sub-interval encoding and decoding. Figure 2a shows the encoding layer that includes excitatory and inhibitory neurons for which the frequency increases with the joint angle α. By analysing the resultant effect of these neurons on the postsynaptic neurons E_i^D, we observed that E_i^D are activated only when α is in the corresponding angle interval $\Delta\alpha_i$. The frequency of the inhibitory neurons I_X is set by adjusting the resistors R_A in order to ensure the activation of E_1^X before E_2^X, and E_2^X before E_3^X when V_J increases. Similarly, a threshold value at which the inhibitory neurons I_i^Y start to activate is set in order to obtain the activation of I_i^Y between E_i^X and E_{i+1}^X. Also, taking into account that E_i^D is inhibited when E_{i+1}^D is activated implies that voltages V_i^X and V_i^Y set the lower and the upper limits of the angle interval $\Delta\alpha_i$ where E_i^D fires, respectively.

3.3. Auxiliary Electronics

The bioinspired system includes several auxiliary electronics that perform the adaptation of the analogue signals generated by the sensors to the input or output of the SNN. The electronics presented in Figure 3 include the angle sensor that generates voltage V_J for the SNN input, as well as the SMA driver that is used to generate the power for the SMA actuators.
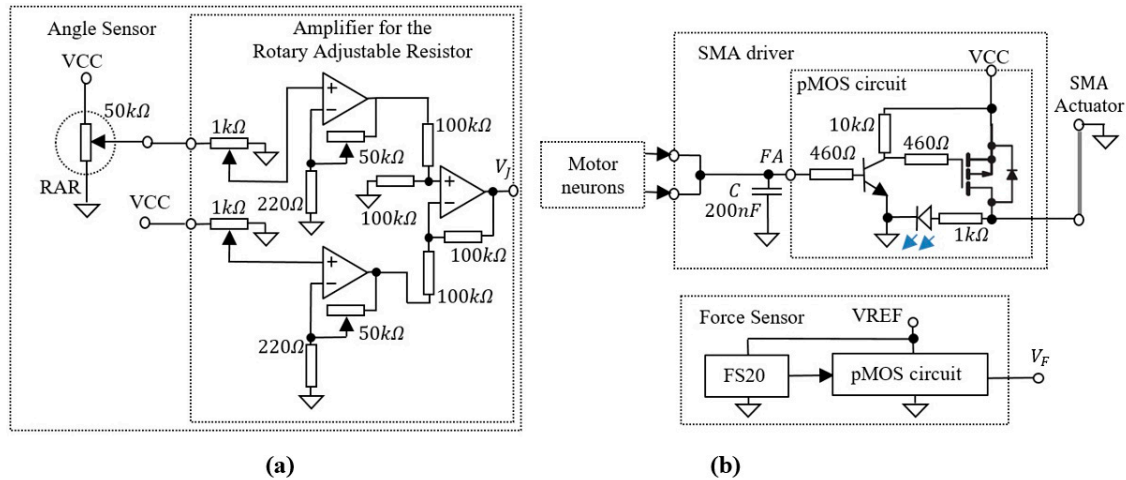

Figure 3. (**a**) Angle sensor including the rotary adjustable resistor and an amplifier; (**b**) SMA driver that integrates the spiking activity of the motor neurons and drives the SMA actuators; A similar pMOS circuit is used to amplify the output of a low force compression load cell FS20.

A similar p-channel MOSFET (pMOS) circuit which is included in the SMA driver is used for output amplification of the compression load cell type FS20.

4. Evaluation by Simulation of the SNN Activity

The main characteristics of the proposed SNN structure (Figure 2) are the ability to encode angles of rotation by the activation of predefined neural paths and the capability to adapt using Hebbian learning mechanisms. This implies that the synaptic weights are potentiated when the untrained neural paths are activated simultaneously with the trained ones. Prior to hardware implementation of the system, we evaluated by simulation in LT Spice the SNN ability to discriminate the voltage intervals and to adapt by Hebbian learning mechanisms. Using the electronic schematic of the hardware neuron (see Figure A1 in the Appendix A), we simulated the neural network presented in Figure 2b to qualify its behaviour. Since the purpose was only to verify the network in a synthetic environment, all the input infrastructure was replaced by signals generated by voltage sources to mimic real scenarios. The voltage V_J was linearly swept through a greater voltage interval that includeed the activation intervals of each excitatory neuron E_i^D. The force sensor output V_F was triggered for one value of V_J in order to activate the learning mechanism. The activation of V_F modeled the presence of an obstacle that pushed on the force sensor in an angle interval. Voltage selectivity was simulated using the potentials V^X and V^Y that represent the output of simulated voltage generators.

Figure 4 shows the results obtained during the simulation of SNN activity when the force sensor was activated concurrently with neuron E_2^D, whose activity simulates the the finger positioning in the angle interval $\Delta\alpha_2$. The upper signals represent the activity of the excitatory neurons E_1^D, E_2^D and E_3^D (Figure 2b) that stimulate the corresponding postsynaptic inhibitory neurons I_1, I_2 and I_3 for which the input is shown by the lower signals.
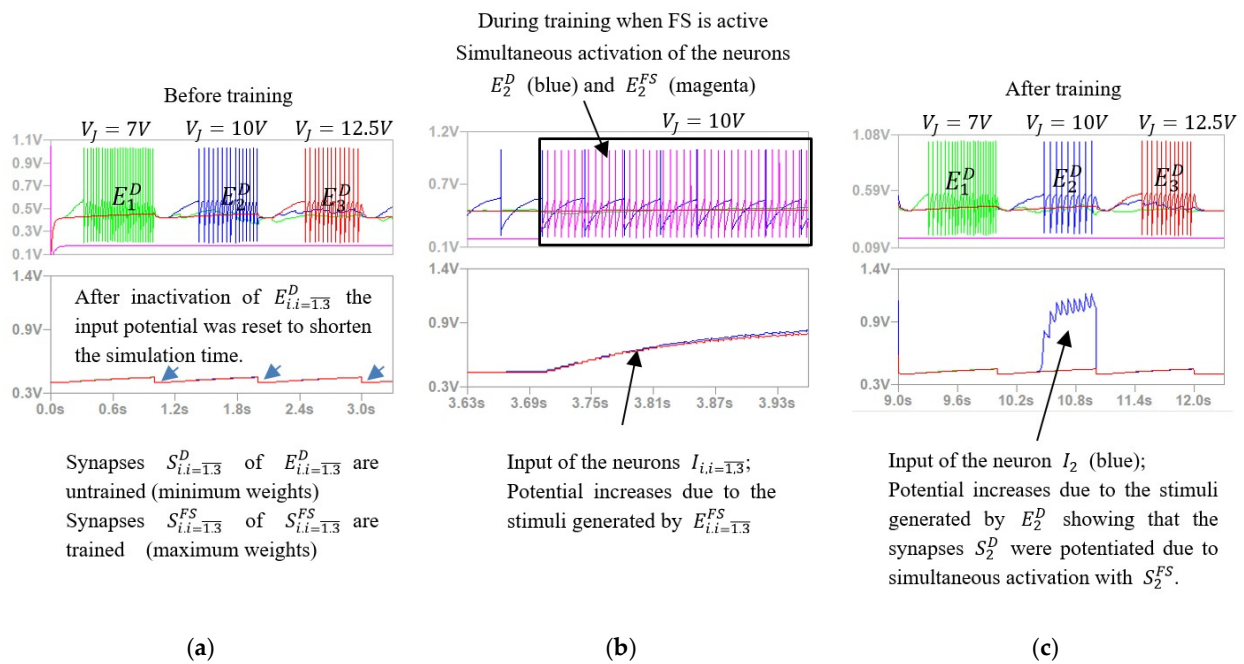
Figure 4. Simulation results showing: (**a**) the activity of the excitatory neurons E_1^D, E_2^D and E_3^D (green, blue, and red signals) that respond to predefined voltage levels corresponding to the angle intervals; (**b**) a magenta signal showing the activity of the excitatory neurons that are stimulated by the force sensor (**c**) neuron activity after training, showing the effect of the potentiated synapses that were activated simultaneously with the force sensor.

Note that, the activation of the neurons E_i^D depends on the value of V_J, implying that the SNN can discriminate between angle intervals (Figure 4a,c). Moreover, as presented in Figure 4c, after training, the stimulation of the neuron I_2 by the neuron E_2^D was significantly stronger than the stimulation of I_1 and I_3 by E_1^D and E_3^D, respectively. This shows that the concurrent activation of neurons E_2^D and E_2^{FS} (Figure 4b) potentiates only the synapses S_2^D, while the weights of S_1^D and S_3^D remained low.

5. Experimental Investigation

The simulation results illustrate that the SNN behaved as expected, allowing us to test these abilities in hardware, as well as the performance of the SNN in stopping the finger in the corresponding angle interval after training.

5.1. Experimental Setup

Figure 5 shows the structure of the bioinspired system including the adaptive SNN that was able to detect the presence of the potential V_J (generated by the angle sensor) in three different voltage intervals and to learn which neural path fired when the force sensor was active. The SNN controlled the actuators through the SMA driver and received information about the rotation of the artificial finger from the RAR amplifier and about the applied force on the finger apex from the CLC pMOS (Figure 3b).

The artificial finger was flexed by an 82 cm-long SMA Flexinol 0.006″-type actuator for which the maximum load was 321 g at 410 mA and cooling time was 2 s. The reference voltages for the SNN are $V_{EQU} = 0.4$ V and $V_{REF} = 5$ V, the later potential being used also to power the force sensor. The supply voltage for the neurons was $VDD = 1.6$ V, while the SMA actuators and angle sensor were powered by $VCC = 14$ V. During the experiments, the room temperature was about 23 °C.
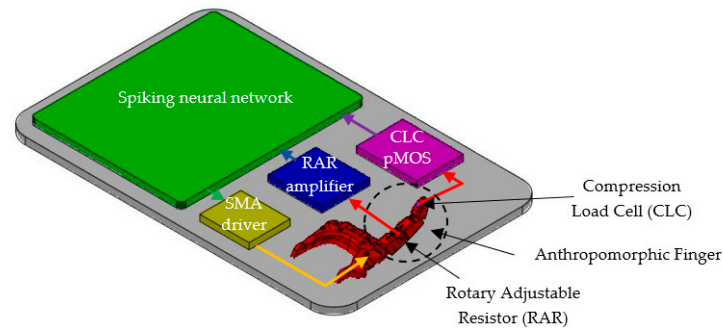
Figure 5. Experimental setup showing the structure of the bioinspired system which includes the spiking neural network, the artificial finger, and auxiliary electronics (SMA driver, RAR amplifier and the CLC pMOS).

5.2. Experiments Overview

The main characteristics of the SNN that were tested in the next were angle interval selectivity and SNN adaptability by associative learning mechanisms. For the selectivity evaluation we monitored the activity of neurons E_1^X, I_1^Y, and I_2^X, included in the sub-SNN which was used to detect the finger in the angle interval $\Delta\alpha_1$. When V_J was in the potential variation range for $\Delta\alpha_1$ the sub-SNN output was activated. Also, we monitored the activity of neurons E_2^D and E_3^D when V_J took several values in the corresponding intervals $\Delta\alpha_2$, $\Delta\alpha_3$ and, respectively, the transition between them.

SNN adaptability was evaluated by monitoring V_J and the activity of neurons E^D, I, and E^{FS} when the finger was actuated. Before training, no inhibition occurred, and during training, the neuron activity showed that the finger pushed on the obstacle rhythmically. After training, E^D activates the postsynaptic neurons I in the absence of the obstacle, stopping the finger. Also, we showed that the inhibitory neurons I_1, I_2, and I_3 were able to independently stop the finger rotation at different angles of rotation.

5.3. Experimental Results

Considering that angle α directly determines the voltage V_J generated by the angle sensor, we evaluated the function $V_J(\alpha)$ experimentally which is plotted in Figure 6.
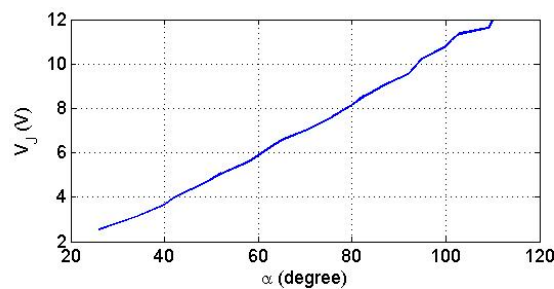

Figure 6. The function $V_J(\alpha)$ generated by the angle sensor.

Considering that the linearity of the function $V_J(\alpha)$ is high, we will refer below only to the voltage V_J in order to simplify the presentation of the results. Thus, the angle intervals $\Delta\alpha_{1-3}$, correspond to the voltage intervals ΔV_{1-3} of the voltage V_J.

5.3.1. Voltage Interval Selectivity

To evaluate the response of the neurons to V_J, the variation of the finger was positioned by an external force in ΔV_1. Figure 7 presents the electronic neuron activity for several values of V_J which were chosen to highlight the SNN ability to detect that V_J was in ΔV_1. Note that the spikes on the diagrams represent electronic neuron activations and the signals represent the potential V_M recorded using a TDS2024 oscilloscope in node (M) of the neuron's schematic (see Appendix A). In Figure 7a, the excitatory neuron E_1^X determines

the activation of E_1^D in the absence of inhibition produced by the neurons I_1^Y and I_2^X. As the inhibitory activity becomes stronger, the frequency of E_1^D reduces (Figure 7b) until it is fully inhibited, as in Figure 7c.
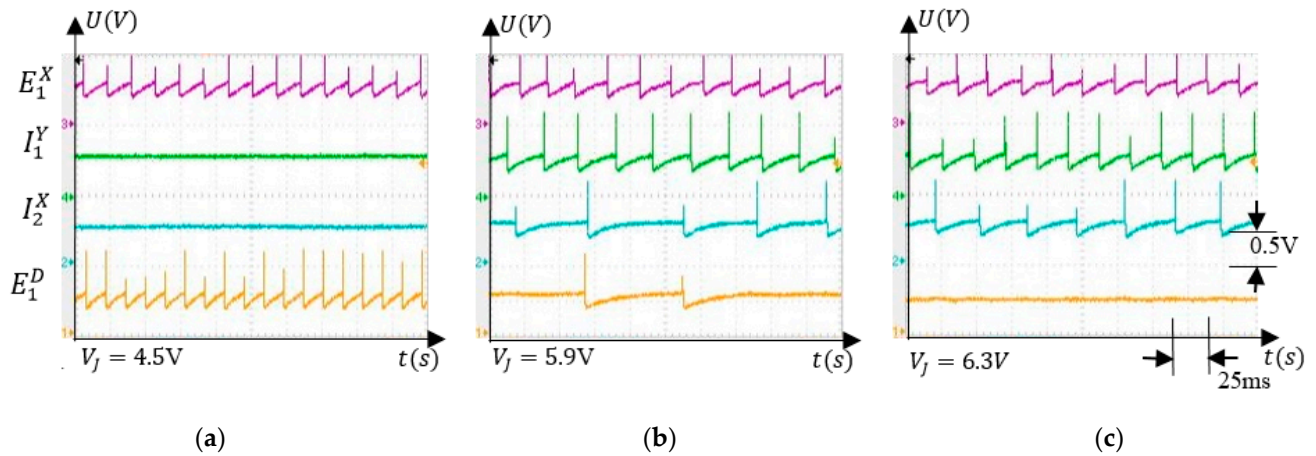

Figure 7. Activity of the neurons that stimulate E_1^D when V_J takes several values; (**a**) no inhibition; (**b**) partial inhibition; (**c**) ful inhibition.

The ability of the SNN to activate neural paths that are specific to the values of the input voltage is highlighted by the signals shown in Figure 8. The full activation of neurons, E_2^D and E_3^D occurs when $V_J = 6.5$ V (Figure 8a) and $V_J = 11.1$ V (Figure 8c), respectively.
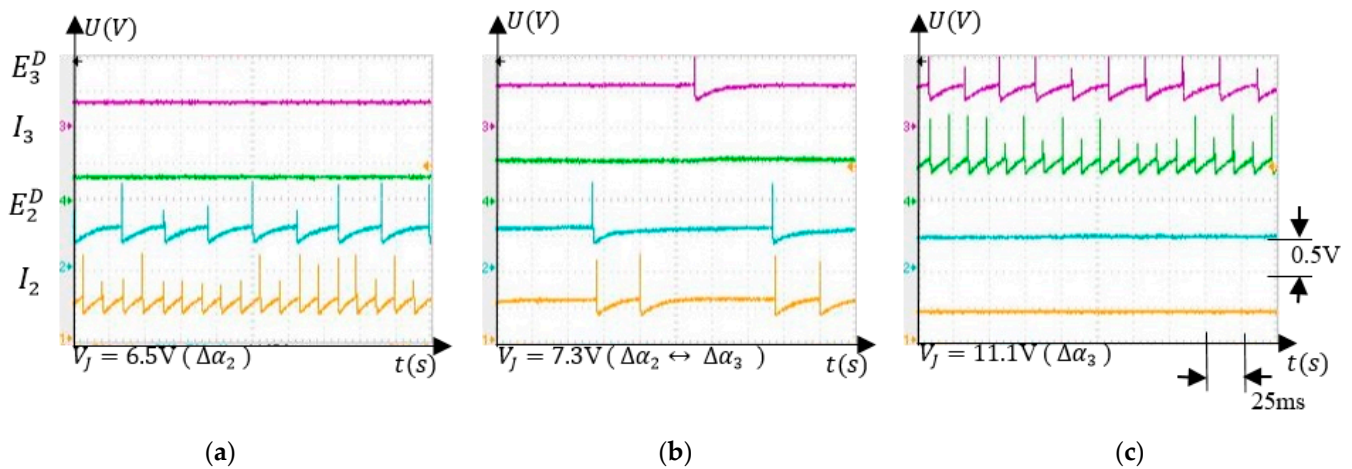

Figure 8. Neuron activity that shows the ability of the SNN to select which neural path to activate according to V_J: (**a**) E_2^D and I_2 activated when the finger is in $\Delta\alpha_2$; (**b**) neurons from both neural paths are activated when the finger is between $\Delta\alpha_2$ and $\Delta\alpha_3$; (**c**) E_3^D and I_3 are activated when the finger is in $\Delta\alpha_3$.

Taking into account that V_J is generated by the angle sensor, the activation of E_2^D and E_3^D signal the presence of the finger in the angle intervals $\Delta\alpha_2$ and $\Delta\alpha_3$, respectively. When signal V_J crosses between thevintervals ΔV_2 and ΔV_3, both E_2^D and E_3^D are activated at a lower frequency.

5.3.2. Associative Learning

The main feature of the SNN is the ability to adapt to activate the corresponding neuron I_i, $i = \overline{1,3}$, which inhibits motor neurons $M_{1,2}$, stopping the finger's rotation (Figure 2b). Learning occurs by long term potentiation when the unpotentiated synapses S_i^D are activated simultaneously with the potentiated synapses S_i^{FS} that activate I_i. Therefore, the SNN training consisted of potentiating the excitatory synapses S_i^D that connect the

neurons E_i^D to the inhibitory neurons I_i^D. The weights of S_i^D increase when the force sensor is activated if the finger is in the corresponding angle interval. An example of the neuron activity when the force sensor is activated by an obstacle in the interval $\Delta\alpha_1$ is shown in Figure 9. Before the training, neuron E_1^D detected that the finger crosses the corresponding angle interval without stopping it (Figure 9a). As shown in Figure 9b, during training, the neuron I_1 is activated only by E_1^{FS} and not by E_1^D, which fires continuously because the finger is stopped in $\Delta\alpha_1$. The activity of neuron E_1^{FS} alternates with silent periods, showing that the SNN has a regulatory behaviour consisting of trying to push on the obstacle.
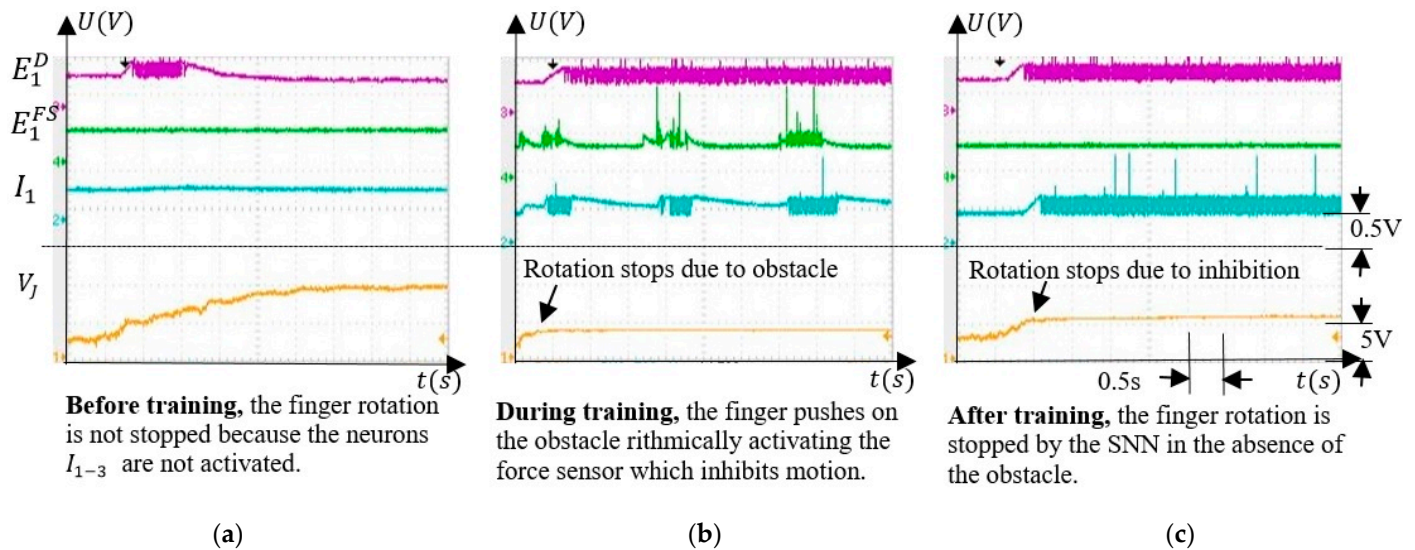

Before training, the finger rotation is not stopped because the neurons I_{1-3} are not activated.

(**a**)

During training, the finger pushes on the obstacle rithmically activating the force sensor which inhibits motion.

(**b**)

After training, the finger rotation is stopped by the SNN in the absence of the obstacle.

(**c**)

Figure 9. (**a**) Before training, neuron E_1^D detects the presence of the finger in the corresponding angle interval; (**b**) during training, neuron E_1^D is activated simultaneously with the neuron E_1^{FS} activating the neuron I_1; (**c**) after training, neuron E_1^D activates inhibitory neuron I_1 stopping the finger rotation without the activity of the E_1^{FS} neurons.

After training, the force sensor remained inactive because the obstacle was removed implying that the neuron E_1^{FS} was silent, as presented in Figure 9c. The neuron I_1 was activated only by the neuron E_1^D through the potentiated synapses S_1^D. Denoting the potential where the finger was stopped by the external force as V_J^{EF}, and the value where the finger stops due to inhibition after training as V_J^{INH}, one can observe that $V_J^{EF} \neq V_J^{INH}$.

This occurs because the finger can be stopped by an obstacle anywhere in the angle interval, but the SNN will stop the finger where the inhibitory activity of I_1 compensates for the excitatory output of neurons $E_{1,2}^{ES}$ (Figure 2b).

5.3.3. Finger Operation

To test the behaviour of the SNN when the finger was rotated, we focused on the independent activity of the inhibitory neurons I_{1-3}. when only one of these neurons fires. First, we tested if the SNN was able to discriminate the angle intervals $\Delta\alpha_{1-3}$ when the finger was actuated by an external force, as presented in Figure 10a. Second, the weights were set to their minimum values when the inhibitory neurons were not sensitive to the finger rotation as in Figure 10b. Figure 11 presents the activity of the inhibitory neurons when only the synapses S_i^D were trained.
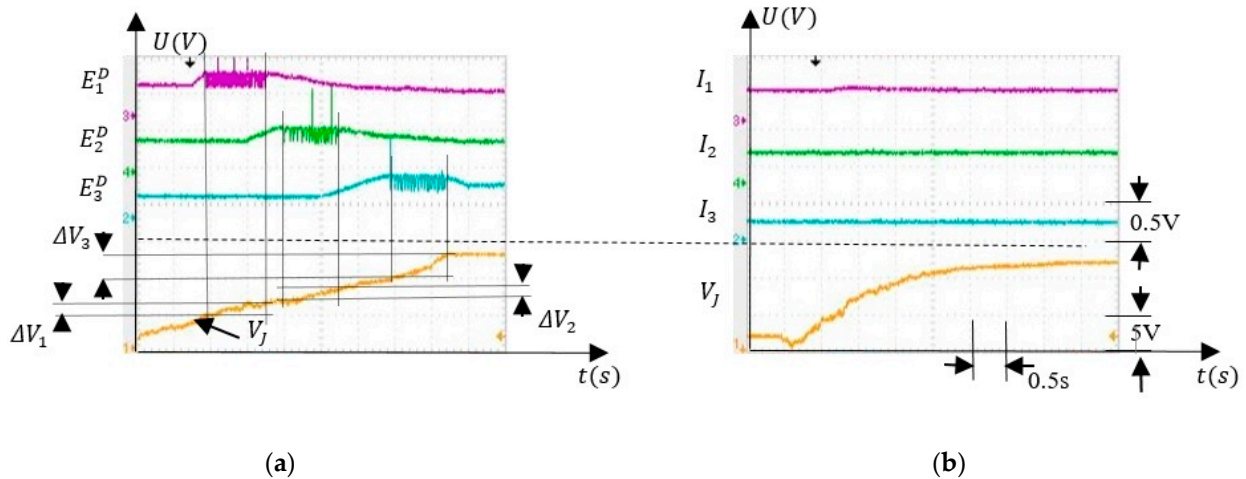
(**a**)

(**b**)

Figure 10. The activity of the critical neurons before training showing the angle interval selection; (**a**) E^D_{1-3} when the artificial finger was rotated by the hand; (**b**) I_{1-3} when the SMA actuator rotated the finger.
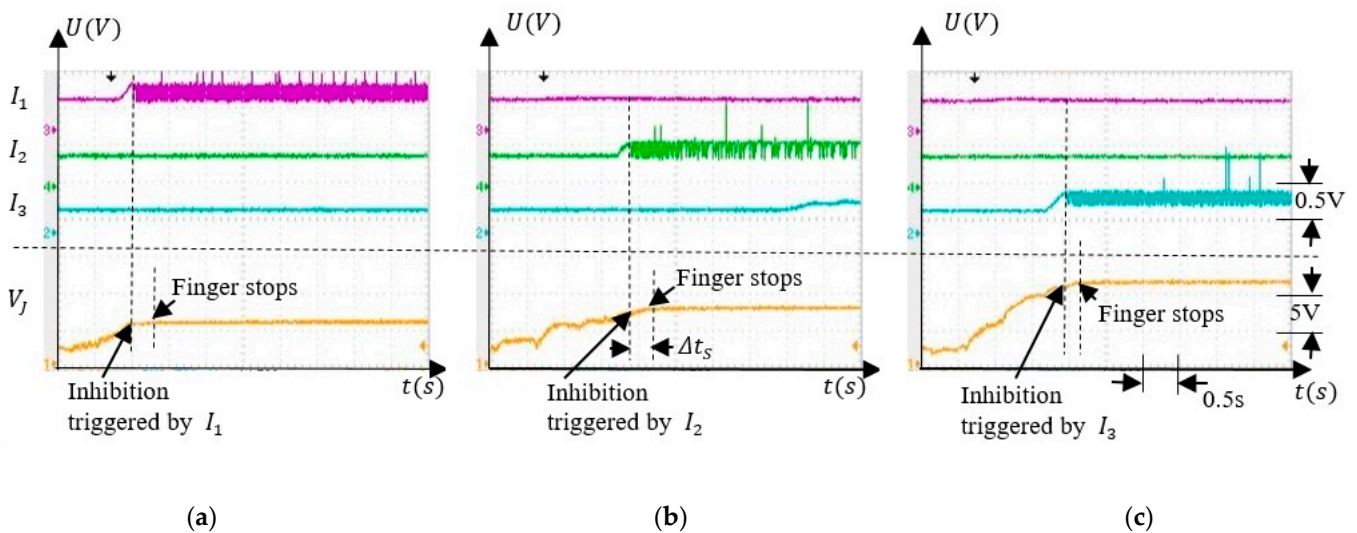

(**a**)

(**b**)

(**c**)

Figure 11. The activity of the inhibitory neurons I_{1-3} stops the finger rotation at angle α corresponding to the values of V_J: (**a**) I_1; (**b**) I_2; and (**c**) I_3.

Note that the potential V_J remains stable shortly after activation of I_i, implying that the finger stopped in the interval $\Delta\alpha_i$, where the force sensor was activated during training. The values where V_J remained constant depended on which inhibitory neuron was activated. Considering that V_J was constant when the rotation was stopped, implies that the corresponding angle α_i depended on the activated neurons I_i, as expected. Also, there is was a Δt_S delay between the activation of the inhibitory neurons and the moment at which the rotation stopped which was determined by the cooling time of the SMA actuator.

5.4. Discussions

The results show that the SNN was able to rigorously discriminate several voltage intervals of the input by balancing the activity of the excitatory and inhibitory neurons despite the oscillations of the finger speed. Also, using few neurons, the SNN learned to activate the inhibitory neurons according to the angle interval where the finger was stopped by the external force. In this work, we did not focus on the precision and accuracy of the finger positioning because these parameters were analysed previously using a similar system based on SNN and SMA actuators [17]. Also, the SNN was not able to stop the finger exactly at the same angle at which it was blocked by the obstacle because the angle

intervals considered were wide. The performance of the finger positioning can be increased by narrowing the angle intervals that can be obtained using more neurons. Theoretically, the minimum width of the angle intervals $\Delta \alpha_{min}$ increases with the rotation speed of the finger joint, implying that lower speeds allow better resolution. As an example, when the rotation speed is 40 $^\circ$/s, the maximum rotation range of $\alpha_{range} = 120^\circ$ is covered by the finger in 3 s. By increasing the number of inhibitory neurons and by significantly reducing the cooling time of the SMA actuator (using water with glycol), the finger can stop when the inhibitory neurons fire once. The simulations of the SNN activity show that the minimum variation of V_J that activates the inhibitory neurons once is $\Delta V_{min} = 0.25$ V, which corresponds to $\Delta \alpha_{min} = 5.8^\circ$. This implies that the maximum number of intervals that cover α_{range} is about $n_{max} = 20$.

The SNN performance was evaluated when the finger was flexed. Knowing that the inhibitory neurons fire when the finger is positioned in the corresponding angle interval independent of the previous one, we can consider that associative learning and inhibition also occur when the finger is rotated in the opposite direction.

Another observation is related to the position of the obstacle at the edge of the angle intervals. In this setup, the intervals $\Delta \alpha_{1-3}$ are disjunctive, implying that both neurons E_i^D and E_{i+1}^D fire at a lower frequency when the finger crosses from $\Delta \alpha_i$ to $\Delta \alpha_{i+1}$ (Figure 8b). This behaviour of the SNN reduces the learning rate, implying that in this uncertainty case, the synapses potentiation is insignificant. However, the intersection of the intervals $\Delta \alpha_i$ and $\Delta \alpha_{i+1}$ can be obtained by making the activation of the neurons E_i^X and I_i^X independent (see Figure 2a) and by setting accordingly the intervals limits. When the obstacle is placed at the intersection of $\Delta \alpha_i$ and $\Delta \alpha_{i+1}$, both E_i^D and E_{i+1}^D activate, potentiating S_i^D, and S_{i+1}^D will stop the arm in the first interval that is reached, reducing the positioning resolution to half.

6. Conclusions

The experiments demonstrate that a bioinspired control system based on an adaptive neural structure of biological inspiration and contractile SMA actuators is sensitive to the rotation angle of an anthropomorphic finger. This is achieved by the activation of different neural paths for different values of the input potential that correspond to several angle intervals. When a supraliminar stimulus activates all neurons that inhibit the output, and thus stopping the rotation, the SNN learns to determine which angle detection neural path (ADNP) was active. This adaptation mechanism connects the ADNP to one inhibitory neuron that stops the rotation in the absence of the supraliminar stimulus. Taking into account the high level of bioinspiration given by the spiking neural structures that control the contractile actuators, this concept can be used to understand how the automatic motions are gained in the basal ganglia. Also, anthropomorphic robots that learn motions based on biological principles could benefit from this concept. Another advantage of this system is the implementation of a spiking neural network in analogue hardware that allows for the control of multiple actuators in parallel without affecting the real-time response of the system.

As a short-term goal, we will comparatively evaluate the performance of SNN and microcontrollers in controlling in parallel the SMA actuated junctions of an anthropomorphic hand for showing in which conditions SNN represents a more advantageous control method. Another future direction is to design a neuron model with an improved learning mechanism in terms of biological rigor and to implement it on an FPGA, which simplifies the prototyping of the future SNN structures.

Author Contributions: Neural network conceptualization: M.H.; robotics conceptualization: C.F.C. and G.I.U.; methodology: M.H. and G.I.U.; simulations: G.I.U.; validation: M.H. and C.F.C.; hardware implementation: M.H. and G.I.U.; investigation: M.H. and G.I.U.; resources: M.H.; writing—original draft preparation: M.H. and G.I.U.; writing—review and editing: C.F.C.; supervision: M.H. All authors have read and agreed to the published version of the manuscript.

Institutional Review Board Statement: Not applicable.

Informed Consent Statement: Not applicable.

Data Availability Statement: Not applicable.

Conflicts of Interest: The authors declare no conflict of interest.

Appendix A

Figure A1 presents the schematic circuit of the electronic neuron that is implemented in PCB hardware [10,11]. The neuron includes one electronic soma (SOMA) and one or more electronic synapses (SYN). The SOMA detects neuron activation threshold using the transistor T_1 and activates the SYNs. As presented in Figure A1a the SOMA of the input neurons which are connected directly to the analogue signals (V^X_{1-3}, V^Y_{1-3}, V_F, V_J and V_{ES} in Figure 3) includes the pair R_E–D_E that determine the oscillation of the neuron with frequency f that depends on the input potential. The SOMA of the postsynaptic neurons which are stimulated by the excitatory or inhibitory synapses includes the pair C_I–R_I which integrates the input activity. When the SOMA activates the connected SYNs, S_{OUT} generates pulses at their output N_{OUT}, whose energy depends on the charge stored in the weight capacitor C_L. Note that the potential V_M was monitored using the oscilloscope in node (M) for visualization of the neuron activations, which are represented by the spikes. Depending on the position of switch S, the generated pulses can be excitatory with maximum amplitude VDD, or inhibitory with minimum amplitude GND (see Figure A1b).

The parameters of the electronic neuron (SOMA and SYN) that were used in the experiments are given in the Tables A1 and A2.
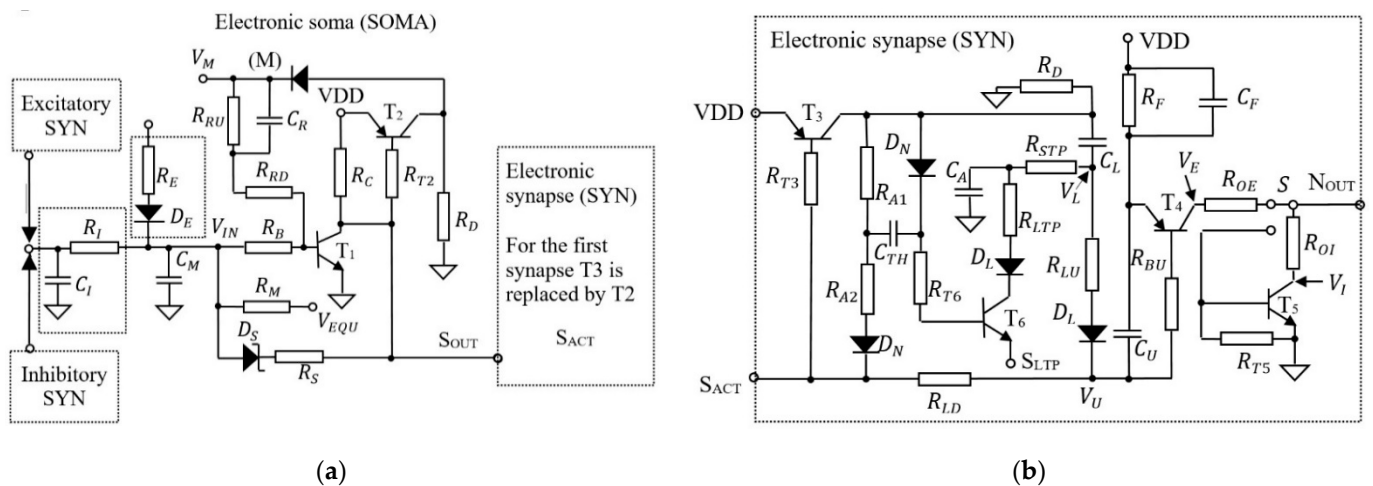

(a)

(b)

Figure A1. The schematic of: (**a**) the electronic SOMA; (**b**) the electronic synapse (SYN) [11].

Table A1. Parameters for the SOMA.

Param.	Value	Param.	Value
R_{RU}	20 kΩ	T_1	BC848C
R_{RD}	1 kΩ	T_2	BC857C
R_{IN}	220 kΩ	D_S	BAR43
R_B	6.2 kΩ	D_N	1N4148
R_C	10 kΩ	D_L	BAS45A
R_D	1 MΩ	C_R	10 nF
R_M	1 MΩ	C_I	1 µF
R_S	47 Ω	C_M	100 nF
R_{T2}	10k Ω		

Table A2. Parameters for the SYN.

Param.	Value	Param.	Value
R_D	1 MΩ	C_{TH}	10 nF
R_F	47 kΩ	C_A	47 nF
R_{T3}	10 kΩ	C_L	2.2 μF
R_{A1}	10 kΩ	C_U	221 pF
R_{A2}	1 kΩ	C_F	1 μF
R_{T6}	470 Ω	T_3	BC857C
R_{STP}	10 kΩ	T_4	BC857C
R_{LTP}	470 Ω	T_5	BC848C
R_{OE}	1.8 kΩ	D_N	1N4148
R_{LU}	1 MΩ	D_L	BAS45A
R_{LD}	470 kΩ	R_E	560 kΩ
R_{BU}	10 kΩ	R_A	5 kΩ
R_{OI}	470 Ω		
R_{T5}	47 kΩ		

References

1. Bing, Z.; Meschede, C.; Röhrbein, F.; Huang, K.; Knoll, A.C. A survey of robotics control based on learning-inspired spiking neural networks. *Front. Neurorobot.* **2018**, *12*, 35. [CrossRef]
2. Al-Falahe, N.A.; Nagaoka, M.; Vallbo, A.B. Response profiles of human muscle afferents during active finger movements. *Brain* **1990**, *113*, 325–346. [CrossRef] [PubMed]
3. Hulliger, M. The mammalian muscle spindle and its central control. *Rev. Physiol. Biochem. Pharmacol.* **1984**, *101*, 1–110. [PubMed]
4. Blum, K.P.; Lamotte D'Incamps, B.; Zytnicki, D.; Ting, L.H. Force encoding in muscle spindles during stretch of passive muscle. *PLoS Comput. Biol.* **2017**, *13*, e1005767. [CrossRef] [PubMed]
5. Peters, R.; Dalton, B.; Blouin, J.-S.; Inglis, T. Precise coding of ankle angle and velocity by human calf muscle spindles. *Neuroscience* **2017**, *349*, 98–105. [CrossRef]
6. Vallbo, A.B. Afferent discharge from human muscle spindles in non-contracting muscles. Steady state impulse frequency as a function of joint angle. *Acta Psychiatr. Scand.* **1974**, *90*, 303–318. [CrossRef] [PubMed]
7. Vallbo, A.B.; Al-Falahe, N.A. Human muscle spindle response in a motor learning task. *J. Physiol.* **1990**, *421*, 553–568. [CrossRef]
8. Dimitriou, M. Enhanced muscle afferent signals during motor learning in humans. *Curr. Biol.* **2016**, *26*, 1062–1068. [CrossRef]
9. Grillner, S.; Robertson, B.; Kotaleski, J.H. Basal ganglia—A motion perspective. *Compr. Physiol.* **2020**, *10*, 1241–1275.
10. Hulea, M. Analogue Electronic Circuit for Implementation of an Artificial Neuron. Patent RO126249 (A2), 29 June 2018.
11. Hulea, M.; Ghassemlooy, Z.; Rajbhandari, S.; Younus, O.I.; Barleanu, A. Optical axons for electro-optical neural networks. *Sensors* **2020**, *20*, 6119. [CrossRef]
12. Lester, B.; Baxevanis, T.; Chemisky, Y.; Lagoudas, D. Review and perspectives: Shape memory alloy composite systems. *Acta Mech.* **2015**, *226*, 3907–3960. [CrossRef]
13. Mohd, J.; Leary, J.M.; Subic, A.; Gibson, M. A review of shape memory alloy research, applications and opportunities. *Mater. Des.* **2014**, *56*, 1078–1113. [CrossRef]
14. Coral, W.; Rossi, C.; Colorado, J.; Barrientos, A. SMA-Based Muscle-Like Actuation in Biologically Inspired Robots: A State of the Art Review. In *Smart Actuation and Sensing Systems–Recent Advances and Future Challenges*; IntechOpen: London, UK, 2012; pp. 52–82.
15. Hulea, M.; Caruntu, C.F. Spiking Neural Network for Controlling the Artificial Muscles of a Humanoid Robotic Arm. In Proceedings of the 18th Conference on System Theory, Control and Computing, Sinaia, Romania, 17–19 October 2014; pp. 163–168.
16. Hulea, M. Bio-Inspired Control Method Based on Spiking Neural Networks and SMA Actuator Wires for LASER Spot Tracking. In *Nature-Inspired Computing for Control Systems*; Hiram, P., Ed.; Springer International Publishing: Cham, Switzerland, 2015; pp. 13–38.
17. Hulea, M.; Burlacu, A.; Caruntu, C.F. Intelligent motion planning and control for robotic joints using bio-inspired spiking neural networks. *Int. J. Hum. Robot.* **2019**, *16*, 1950012. [CrossRef]
18. Quintanar-Guzmán, S.; Kannan, S.; Olivares-Mendez, M.A.; Voos, H. Lightweight Robotic Arm Actuated by Shape Memory Alloy (SMA) Wires. In Proceedings of the 2016 8th International Conference on Electronics, Computers and Artificial Intelligence, Ploiesti, Romania, 30 June–2 July 2016.
19. Grillner, S. The motor infrastructure from ion channels to neuronal networks. *Nat. Rev. Neurosci.* **2003**, *4*, 573–586. [CrossRef] [PubMed]
20. Hulea, M.; Uleru, G.; Burlacu, A.; Caruntu, C. Bioinspired SNN for Robotic Joint Control. In Proceedings of the IEEE International Conference on Automation, Quality and Testing, Robotics, Cluj-Napoca, Romania, 21–23 May 2020; pp. 1–5.

21. Golgouneh, A.; Holschuh, B.; Dunne, L. A Controllable Biomimetic SMA-Actuated Robotic Arm. In Proceedings of the 2020 8th IEEE RAS/EMBS International Conference for Biomedical Robotics and Biomechatronics, New York, NY, USA, 29 November–1 December 2020.

22. Vasquez Tieck, J.C.; Donat, H.; Kaiser, J.; Peric, I.; Ulbrich, S.; Roennau, A.; Zöllner, M.; Dillmann, R. Towards Grasping with Spiking Neural Networks for Anthropomorphic Robot Hands. In *Lecture Notes in Computer Science*; Springer: Cham, Switzerland, 2017; Volume 10613, pp. 43–51.

23. Arena, P.; De Fiore, S.; Patané, L.; Pollino, M.; Ventura, C. STDP-based behavior learning on the TriBot robot. In Proceedings of the Bioengineered and Bioinspired Systems IV, Dresden, Germany, 20 May 2009.

24. Andrianesis, K.; Tzes, A. Development and control of a multifunctional prosthetic hand with shape memory alloy actuators. *J. Intell. Robot. Syst.* **2014**, *78*, 257–289. [CrossRef]

25. Ulloa, C.C.; Terrile, S.; Barrientos, A. Soft underwater robot actuated by shape-memory alloys jellyrobcib for path tracking through fuzzy visual control. *Appl. Sci.* **2020**, *10*, 7160. [CrossRef]

26. Garcia-Cordova, F.; Lopez-Coronado, J.; Guerrero-Gonzalez, A. Design of an Anthropomorphic Finger Using Shape Memory Alloy Springs. In Proceedings of the IEEE International Conference on Systems, Man, and Cybernetics (Cat. No.99CH37028), Tokyo, Japan, 12–15 October 1999; pp. 794–799.

27. Sugita, K.; Tanaka, D.; Ono, S.; Chiba, S.; Iwata, K.; Han, Y.; Takato, M.; Uchikoba, F.; Saito, K. SMA Actuator and Pulse-Type Hardware Neural Networks IC for Fast Walking Motion of Insect-Type MEMS Microrobot. In Proceedings of the IEEE International Conference on Advanced Intelligent Mechatronics, Banff, AB, Canada, 12–15 July 2016; pp. 431–435.

28. Brailovski, V.; Terriault, P.; Georges, T.; Coutu, D. SMA actuators for morphing wings. *Phys. Procedia* **2010**, *10*, 197–203. [CrossRef]

29. Koh, J.-S.; Kim, S.-W.; Noh, M.; Cho, K.-J. Biologically inspired robots using Smart Composite Microstructures. In Proceedings of the 8th International Conference on Ubiquitous Robots and Ambient Intelligence, Incheon, Korea, 23–26 November 2011; p. 871.

30. Yu, Q.; Ma, C.; Song, S.; Zhang, G.; Dang, J.; Tan, K. Constructing Accurate and Efficient Deep Spiking Neural Networks with Double-threshold and Augmented Schemes. *arXiv* **2020**, arXiv:2005.03231.

31. Taherkhani, A.; Belatreche, A.; Li, Y.; Cosma, G.; Maguire, L.; McGinnity, T.M. A Review of Learning in Biologically Plausible Spiking Neural Networks. *Neural Netw.* **2020**, *122*, 253–272. [CrossRef]

32. López, L.J.; Del Ser, J.; Bifet, A.; Kasabov, N. Spiking Neural Networks and online learning: An overview and perspectives. *Neural Netw.* **2020**, *121*, 88–100.

33. Wang, X.; Lin, X.; Dang, X. Supervised learning in spiking neural networks: A review of algorithms and evaluations. *Neural Netw.* **2020**, *125*, 258–280. [CrossRef]

34. Kim, J.; Kim, K.; Kim, J. Unifying Activation- and Timing-based Learning Rules for Spiking Neural Networks. *arXiv* **2020**, arXiv:2006.02642.

35. Hao, Y.; Huang, X.; Dong, M.; Xu, B. A biologically plausible supervised learning method for spiking neural networks using the symmetric STDP rule. *Neural Netw.* **2019**, *121*, 387–395. [CrossRef] [PubMed]

36. Lobov, S.A.; Mikhaylov, A.N.; Shamshin, M.; Makarov, V.A.; Kazantsev, V.B. Spatial Properties of STDP in a Self-Learning Spiking Neural Network Enable Controlling a Mobile Robot. *Front. Neurosci.* **2020**, *14*, 88. [CrossRef]

37. Demin, V.; Nekhaev, D.; Surazhevsky, I.A.; Nikiruy, K.; Emelyanov, A.; Nikolaev, S.; Rylkov, V.; Kovalchuk, M.V. Necessary conditions for STDP-based pattern recognition learning in a memristive spiking neural network. *Neural Netw.* **2020**, *134*, 64–75. [CrossRef]

38. Shi, M.; Zhang, T.; Zeng, Y. Corrigendum: A Curiosity-Based Learning Method for Spiking Neural Networks. *Front. Comput. Neurosci.* **2020**, *14*, 7. [CrossRef] [PubMed]

39. Shim, Y.; Philippides, A.; Staras, K.; Husbands, P. Unsupervised Learning in an Ensemble of Spiking Neural Networks Mediated by ITDP. *PLoS Comput. Biol.* **2016**, *12*, e1005137. [CrossRef] [PubMed]

40. Qu, L.; Zhao, Z.; Wang, L.; Wang, Y. Efficient and hardware-friendly methods to implement competitive learning for spiking neural networks. *Neural Comput. Appl.* **2020**, *32*, 13479–13490. [CrossRef]

41. Kumarasinghe, K.; Kasabov, N.; Taylor, D. Deep learning and deep knowledge representation in Spiking Neural Networks for Brain-Computer Interface. *Neural Netw.* **2020**, *121*, 169–185. [CrossRef] [PubMed]

42. Fang, H.; Shrestha, A.; Zhao, Z.; Qiu, Q. Exploiting Neuron and Synapse Filter Dynamics in Spatial Temporal Learning of Deep Spiking Neural Network. In Proceedings of the Twenty-Ninth International Joint Conference on Artificial Intelligence (IJCAI), Yokohama, Japan, 7–15 January 2021.

43. Tang, G.; Kumar, N.; Michmizos, K.P. Reinforcement Co-Learning of Deep and Spiking Neural Networks for Energy-Efficient Mapless Navigation with Neuromorphic Hardware. In Proceedings of the International Conference on Intelligent Robots and Systems (IROS), Las Vegas, NV, USA, 24 January 2021 pp. 6090–6097.

44. Payvand, M.; Fouda, M.E.; Kurdahi, F.; Eltawil, A.; Neftci, E. On-Chip Error-triggered Learning of Multi-layer Memristive Spiking Neural Networks. *IEEE J. Emerg. Sel. Top. Circuits Syst.* **2020**, *10*, 522–535. [CrossRef]

45. Skatchkovsky, N.; Jang, H.; Simeone, O. Spiking Neural Networks—Part II: Detecting Spatio-Temporal Patterns. *IEEE Commun. Lett.* **2021**. [CrossRef]

46. Cheng, X.; Zhang, T.; Jia, S.; Xu, B. Finite Meta-Dynamic Neurons in Spiking Neural Networks for Spatio-temporal Learning. *arXiv* **2020**, arXiv:2010.03140.

47. Baagyere, E.; Moses, A.; Zhen, Q.; Oyetunji, E.; Qin, Z. A Multi-Spiking Neural Network Learning Model for Data Classification. *IEEE Access* **2020**, *8*, 72360–72371.
48. Maciąg, P.; Kryszkiewicz, M.; Bembenik, R.; López, L.J.; Del Ser, J. Unsupervised Anomaly Detection in Stream Data with Online Evolving Spiking Neural Networks. *Neural Netw.* **2019**, *139*, 118–139. [CrossRef] [PubMed]
49. Bullock, D.; Grossberg, S.; Guenther, F.H. A self-organizing neural model of motor equivalent reaching and tool use by a multijoint arm. *J. Cogn. Neurosci.* **1993**, *5*, 408–435. [CrossRef] [PubMed]
50. Bouganis, A.; Shanahan, M. Training a spiking neural network to control a 4-DoF robotic arm based on Spike Timing-Dependent Plasticity. In Proceedings of the 2010 International Joint Conference on Neural Networks, Barcelona, Spain, 18–23 July 2010; pp. 1–8.
51. Shuzhi, S.G.; Hang, C.C.; Woon, L.C. Adaptive neural network control of robot manipulators in task space. *IEEE Trans. Ind. Electron.* **1997**, *44*, 746–752. [CrossRef]
52. Almusawi, A.R.J.; Dülger, L.; Sadettin, K. A new artificial neural network approach in solving inverse kinematics of robotic arm (Denso VP6242). *Comput. Intell. Neurosci.* **2016**, *2016*, 5720163. [CrossRef]
53. Ligutan, D.D.; Abad, A.C.; Dadios, E.P. Adaptive Robotic Arm Control using Artificial Neural Network. In Proceedings of the 2018 IEEE 10th International Conference on Humanoid, Nanotechnology, Information Technology, Communication and Control, Environment and Management, Baguio City, Philippines, 29 November–2 December 2018.
54. Tieck, J.C.V.; Steffen, L.; Kaiser, J.; Roennau, A.; Dillmann, R. Controlling a robot arm for target reaching without planning using spiking neurons. In Proceedings of the 2018 IEEE 17th International Conference on Cognitive Informatics & Cognitive Computing, Berkeley, CA, USA, 16–18 July 2018.
55. Yang, J.; Na, J.; Gao, G.; Zhang, C. Adaptive neural tracking control of robotic manipulators with guaranteed nn weight convergence. *Complexity* **2018**, *2018*, 7131562. [CrossRef]
56. Chadderdon, G.; Neymotin, S.; Kerr, C.; Lytton, W. Reinforcement learning of targeted movement in a spiking neuronal model of motor cortex. *PLoS ONE* **2012**, *7*, e47251. [CrossRef] [PubMed]
57. Chou, T.S.; Bucci, L.D.; Krichmar, J.L. Learning touch preferences with a tactile robot using dopamine modulated STDP in a model of insular cortex. *Front. Neurorobot.* **2015**, *9*, 6. [CrossRef] [PubMed]
58. Tieck, J.C.V.; Becker, P.; Kaiser, J.; Peric, I.; Akl, M.; Reichard, D.; Roennau, A.; Dillmann, R. Learning Target Reaching Motions with a Robotic Arm Using Brain-Inspired Dopamine Modulated STDP. In Proceedings of the 2019 IEEE 18th International Conference on Cognitive Informatics & Cognitive Computing, Milan, Italy, 23–25 July 2019; pp. 54–61.
59. Chakravarthy, S.; Joseph, D.; Surampudi, B. What do the basal ganglia do? A modeling perspective. *Biol. Cybern.* **2010**, *103*, 237–253. [CrossRef] [PubMed]
60. Camilo, V.T.J.; Pogančić, M.V.; Kaiser, J.; Roennau, A.; Gewaltig, M.-O.; Dillmann, R. Learning Continuous Muscle Control for a Multi-joint Arm by Extending Proximal Policy Optimization with a Liquid State Machine. In *Lecture Notes in Computer Science*; Springer: Cham, Switzerland, 2018; Volume 11139.
61. Nichols, E.; McDaid, L.J.; Siddique, N. Biologically Inspired SNN for Robot Control. *IEEE Trans. Cybern.* **2013**, *43*, 115–128. [CrossRef] [PubMed]
62. Clawson, T.S.; Ferrari, S.; Fuller, S.B.; Wood, R.J. Spiking neural network (SNN) control of a flapping insect-scale robot. In Proceedings of the 2016 IEEE 55th Conference on Decision and Control, Las Vegas, NV, USA, 12–14 December 2016; pp. 3381–3388.